Automatic Netlist Extraction for Measurement-Based Characterization of Off-Chip Interconnect

Steven D. Corey and Andrew T. Yang, *Member, IEEE*

***Abstract*—An approach is presented for modeling board-level, package-level, and multichip module (MCM) substrate-level interconnect circuitry based on measured time-domain reflectometry (TDR) data. The time-domain scattering parameters of a multiport system are used to extract a SPICE netlist from standard elements to match the behavior of the device up to a user-specified cutoff frequency. Linear or nonlinear circuits may be connected to the model ports, and the entire circuit simulated in a standard circuit simulator. Two- and four-port microstrip-circuit examples are characterized, and the simulation results are compared with measured data. Delay, reflection, transmission, and crosstalk are accurately modeled in each case.**

***Index Terms*—Circuit modeling, circuit simulation, identification, interconnect modeling, state-space methods.**

I. Introduction

As THE rise times of digital signals enter the subnanosecond range, the effects of off-chip interconnect circuitry become increasingly important. Packaging and board-level circuitry—electrically transparent at low frequencies—can cause delay, crosstalk, and reflection transients. If not considered during the design stage, these effects can render a fabricated circuit inoperable. Cable and backplane connectors can also cause failure at the system level if not taken into account.

Interconnect circuitry has traditionally been characterized for simulation using models composed of standard linear elements derived from circuit materials and geometry. If model topology and element values are well chosen, the model will accurately represent the behavior of the physical circuit within a frequency range. For simple circuits with regular geometries, topology and element values may be determined by inspection or by simple formulas. However, for more complex circuits, automatic extraction is necessary [1], generally by discretization of Maxwell's equations. It is known that an automatically generated netlist can be prohibitively large, even for a circuit of modest physical size, since the circuit must be discretized into pieces smaller than the smallest propagating wavelength of interest. For this reason, methods have been developed [2]–[4] for reducing a large netlist to an approximate low-frequency system if the size of the original netlist is manageable. However, tuning such a reduced circuit to match empirical data is difficult.

Distributed models have been presented as alternatives to lumped-element approximation [5], [6]. These models are generally derived analytically from Maxwell's equations, subject to particular sets of boundary conditions and simplifying approximations. Distributed models allow efficient simulation of specific distributed geometries and may be scaled with geometry, but they are not easily derived for three-dimensional (3-D) circuits with complicated geometry and coupling.

Measurement-based modeling techniques are useful when models based on field solution are difficult or costly to obtain. Several such approaches have been presented to generate SPICE-compatible models for certain types of commonly occurring circuits [7], [8]. Models which allow direct inclusion of measured (or computed) impulse-response data have been proposed to simulate circuits whose characteristics are difficult to describe by analytic or lumped representations. Frequency-domain impulse-response approaches [9] are difficult to extend to the case of arbitrary nonlinear loads, although this was accomplished in [10] via harmonic-balance techniques. Techniques which require full convolution [11] can be computationally expensive if the system impulse-response waveforms are long, although this can be partially remedied by recursive evaluation of the convolution integral [12], [13]. However, any model which directly incorporates impulse-response data into simulation will not consist of standard SPICE elements, and therefore, requires implementation of additional simulation code. Furthermore, because each impulse-response waveform is typically modeled separately, simulation time for an m-port circuit increases as m^2.

This paper presents a verifiable approach for modeling interconnect circuits on printed circuit boards, integrated-circuit (IC) packages, or multichip module (MCM)/hybrid substrates [14], [15]. A subcircuit consisting of standard SPICE elements is automatically extracted from the measured time-domain scattering step-response waveforms of a multiport device under test (DUT). Rigorous treatment of potential ill conditioning in the problem yields a more robust extraction algorithm than presented in [13]. Lumped elements are used to characterize the DUT, and the response of the model is valid up to a specified maximum frequency or minimum risetime on the input signal. As a SPICE subcircuit, the model can be incorporated into a standard simulator and connected by its port nodes to any other SPICE circuit—linear or nonlinear. Because the approach is mathematically general,

Manuscript received January 5, 1997; revised May 22, 1997. This work was supported by the National Science Foundation under Grant MIP 9257279AM04 and by Tektronix.

S. D. Corey is with the Department of Electrical Engineering, University of Washington, Seattle, WA 98195-2500 USA.

A. T. Yang was with the Department of Electrical Engineering, University of Washington, Seattle, WA 98195-2500 USA. He is now with Avant! Coporation, Freemont, CA 94538 USA.

Publisher Item Identifier S 0018-9480(97)07391-2.

linear multiport circuits with arbitrary geometry and cross coupling can be modeled without exact knowledge of their internal characteristics. Furthermore, use of standard SPICE elements ensures compatibility with existing simulation tools. Results of the measurement, characterization, and simulation of two- and four-port microstrip-circuit examples are included in this paper. Comparison between simulation results and measurement show that delay, reflection, and crosstalk are accurately modeled.

II. Background

In the approach presented in this paper, lumped-element models are extracted directly from the measured time-domain response of a circuit. Use of measured data greatly decouples the modeling process from circuit topology and geometry, since the internal structure of the circuit is of secondary importance. Scattering parameters are employed for model formulation since they are measurable at high frequency, and because a scattering impulse response is typically shorter in duration than its admittance or impedance counterpart.

A. Lumped-Element Impulse-Response Approximation

A circuit composed of resistors, inductors, capacitors, and control sources excited separately by an impulse at each port is described by the system of linear first-order constant-coefficient differential equations [16]

$$\mathbf{C}\dot{\mathbf{S}}(t)+\mathbf{G}\mathbf{S}(t)=\delta(t)\mathbf{I}. \tag{1}$$

The $M\times M$ matrices $\mathbf{C}$ and $\mathbf{G}$ are constant, $\mathbf{S}(t)$ is the system impulse response [16], and $\mathbf{I}$ is the $M\times M$ identity matrix. The solution to (1) is

$$\mathbf{S}(t)=e^{\mathbf{X}t}\mathbf{C}^{-1}=e^{\mathbf{X}t}\mathbf{S}(0) \tag{2}$$

where

$$\mathbf{X}=-\mathbf{C}^{-1}\mathbf{G}. \tag{3}$$

In general, the inputs and outputs of the system may represent any set of state variables. If the right-hand side (RHS) of (1) represents incident-voltage waves and $\mathbf{S}(t)$ represents reflected-voltage waves, then $\mathbf{S}(t)$ is the scattering response of the circuit.

An eigendecomposition of $\mathbf{X}$ in (2) shows that if $\mathbf{X}$ is nondefective, each element of $\mathbf{S}(t)$ is a sum of weighted exponentials of the form

$$s_{ij}(t)=k_1e^{p_1t}+,\cdots,+k_Me^{p_Mt} \tag{4}$$

where p_i are the M poles of the network, and the k_i are the residues of the scattering parameter element. If $\mathbf{X}$ is allowed to be defective [16], (2) represents a set of basis functions similar to (4), which can describe any lumped or distributed linear system over a finite frequency range.

B. Impulse-Response Sampling

In this paper, sampled time-domain waveforms are used to generate a SPICE netlist. Equation (2) in the continuous-time domain is related to the sampled-time domain of digitized waveforms by defining

$$\mathbf{S}[n]=\mathbf{S}(nT)=(e^{\mathbf{X}T})^n\mathbf{S}(0)=\mathbf{Q}^n\mathbf{S}[0]. \tag{5}$$

It follows that

$$\mathbf{S}[n+1]=\mathbf{Q}\mathbf{S}[n] \tag{6}$$

$$\mathbf{S}[0]=\mathbf{S}(0)=\mathbf{C}^{-1}. \tag{7}$$

That is, if the initial conditions of the continuous system are set and no excitation is applied, the response at time $T,2T,3T,\cdots,nT,\cdots$, may be determined from the set of difference equations in (6). Furthermore, if the initial conditions are set to $\mathbf{C}^{-1}$, (6) computes samples of the impulse response of the system. In essence, the impulse response $S[n]$ of the discrete system, which is the sampled impulse response of the continuous-time system, is completely described by $\mathbf{Q}$ and $\mathbf{C}$.

Because a complete set of samples of the true impulse response described by (5) cannot be measured due to the finite bandwidth of excitation signals and measurement systems, the samples must be approximated. In this paper, a frequency-domain deconvolution scheme similar to that in [13] was used. More robust de-embedding solutions may be found in the literature [17].

III. Automatic Netlist Extraction

The modeling approach presented in this paper begins with $\mathbf{S}[n]$, which contains samples of the system impulse-response matrix as introduced in Section II. Determination of $\mathbf{Q}$ and $\mathbf{C}$ from this measured data represents an inverse problem, and therefore, tends to be ill conditioned. In this section the problem is formulated, and a well-conditioned approach is presented for its solution.

A. Problem Formulation

It can be seen from (6) and (7) that $\mathbf{Q}$ may be computed from any two consecutive samples of the matrix $\mathbf{S}[n]$, and $\mathbf{C}^{-1}$ may be determined given $\mathbf{Q}$ and a single sample of $\mathbf{S}[n]$. However, since we begin with data measured at the m ports of the DUT, the entire $M\times M$ matrix $\mathbf{S}[n]$ is generally not available. That is, only an $m\times m$ portion of the impulse-response waveforms may be observed at the ports of the DUT, leaving a number of the $s_{ij}[n]$ unknown. These unknown elements are the scattering-parameter waveforms at the so-called *internal* (nonport) nodes. To deal with these unmeasurable entries in $\mathbf{S}[n]$, it is partitioned according to

$$\mathbf{S}[n]=\begin{bmatrix}\mathbf{S}_p[n] & \mathbf{S}_3[n]\\ \mathbf{S}_i[n] & \mathbf{S}_4[n]\end{bmatrix} \tag{8}$$

where $\mathbf{S}_p[n]$, the *port waveforms*, are the $m\times m$ portion of $\mathbf{S}[n]$ that represents the full set of m-port measurements. Only $\mathbf{S}_p[n]$ is known from measurement, whereas the remaining portions of the matrix—the *internal waveforms*—are unknown. Inspection of (6) reveals that the relationship does not require

that $\mathbf{S}[n]$ be an $M \times M$ matrix but that it need only be an $M \times k$ matrix, composed of k columns of $\mathbf{S}[n]$ for any integer $k \leq M$. Therefore, (6) may be reduced to

$$\begin{bmatrix} \mathbf{S}_p[n+1] \\ \mathbf{S}_i[n+1] \end{bmatrix} = \mathbf{Q} \begin{bmatrix} \mathbf{S}_p[n] \\ \mathbf{S}_i[n] \end{bmatrix} \tag{9}$$

and the equality is still satisfied. In order to solve for $\mathbf{Q}$, measured samples are substituted into (9) for various sample points n. The relationship may now be expressed, independent of n as

$$\begin{bmatrix} \mathbf{S}_p[1] & \cdots & \mathbf{S}_p[n-1] \\ \mathbf{S}_i[1] & \cdots & \mathbf{S}_i[N-1] \end{bmatrix} = \mathbf{Q} \begin{bmatrix} \mathbf{S}_p[0] & \cdots & \mathbf{S}_p[N-2] \\ \mathbf{S}_i[0] & \cdots & \mathbf{S}_i[N-2] \end{bmatrix} \tag{10}$$

where N is the number of measurement samples. Again it should be noted that $\mathbf{S}_p[n]$ is known, while $\mathbf{S}_i[n]$ is unknown. For notational convenience, (10) may be restated more concisely as

$$\begin{bmatrix} \mathbf{S}_{1,p} \\ \mathbf{S}_{1,i} \end{bmatrix} = \mathbf{Q} \begin{bmatrix} \mathbf{S}_{0,p} \\ \mathbf{S}_{0,i} \end{bmatrix} \qquad \mathbf{S}_1 = \mathbf{Q}\mathbf{S}_0. \tag{11}$$

However, the matrix $\mathbf{Q}$ is $M \times M$, where M is the order of the system of ordinary differential equations which describes the network, and is therefore, not known at measurement time. Since the dimension of $\mathbf{Q}$ is unknown, the dimension of $\mathbf{S}_i[n]$ in (9) is also unknown. However, because only $\mathbf{S}_p[n]$ (the behavior at the ports of the system) is being modeled, the lower M–m entries in each vector are somewhat arbitrary.

Since the system is being modeled by $\mathbf{Q}$, it is important to keep $\mathbf{Q}$ as small in dimension as possible to minimize model complexity. This is clearly achieved by minimizing the number of rows in $\mathbf{S}_{0,i}$ and $\mathbf{S}_{1,i}$. An eigendecomposition of a nondefective $\mathbf{Q}$ in (5) results in

$$\mathbf{S}[n] = \mathbf{Q}^n \mathbf{C}^{-1} = \mathbf{W} \Lambda^n \mathbf{W}^{-1} \mathbf{C}^{-1} \tag{12}$$

where $\mathbf{W}$ contains the eigenvectors and Λ the eigenvalues of $\mathbf{Q}$. Each element of $\mathbf{S}[n]$, and therefore, the columns of $\mathbf{S}_0$ and $\mathbf{S}_1$, are seen to be linear combinations of the eigenvalues of $\mathbf{Q}$ raised to the power n as follows:

$$s_{ij}[n] = \tilde{k}_1 \lambda_1^n + \cdots + \tilde{k}_M \lambda_M^n \tag{13}$$

where λ_i are the eigenvalues of $\mathbf{Q}$. Since M is the dimension of $\mathbf{Q}$, $\mathbf{S}_{0,i}$ and $\mathbf{S}_{1,i}$ should be chosen so as not to introduce any terms into (13) which are not necessary to model the port waveforms $\mathbf{S}_{0,p}$ and $\mathbf{S}_{1,p}$. In this paper, the scheme used to build $\mathbf{S}_{0,i}$ and $\mathbf{S}_{1,i}$ results in the following system of equations:

$$\begin{bmatrix} \mathbf{S}_p[1] & \cdots & \mathbf{S}_p\left[\frac{N}{2}\right] \\ & \cdots & \\ \mathbf{S}_p\left[\frac{N}{2}\right] & \cdots & \mathbf{S}_p[N-1] \end{bmatrix} = \mathbf{Q}' \begin{bmatrix} \mathbf{S}_p[0] & \cdots & \mathbf{S}_p\left[\frac{N}{2}-1\right] \\ & \cdots & \\ \mathbf{S}_p\left[\frac{N}{2}-1\right] & \cdots & \mathbf{S}_p[N-2] \end{bmatrix}. \tag{14}$$

The matrix $\mathbf{Q}'$ is the variant of $\mathbf{Q}$ corresponding to the particular choice of internal waveforms in (14). Partitioning (14) into port waveforms and internal waveforms in a manner analogous to (10) and (11) results in

$$\begin{bmatrix} \mathbf{S}'_{1,p} \\ \mathbf{S}'_{1,i} \end{bmatrix} = \mathbf{Q}' \begin{bmatrix} \mathbf{S}'_{0,p} \\ \mathbf{S}'_{0,i} \end{bmatrix} \qquad \mathbf{S}'_1 = \mathbf{Q}'\mathbf{S}'_0 \tag{15}$$

where

$$\mathbf{S}'_{0,p} = \begin{bmatrix} \mathbf{S}_p[0] & \mathbf{S}_p[1] & \cdots & \mathbf{S}_p\left[\frac{N}{2}-1\right] \end{bmatrix}$$
$$\mathbf{S}'_{1,p} = \begin{bmatrix} \mathbf{S}_p[1] & \mathbf{S}_p[2] & \cdots & \mathbf{S}_p\left[\frac{N}{2}\right] \end{bmatrix}. \tag{16}$$

The internal waveforms $\mathbf{S}'_{0,i}$ and $\mathbf{S}'_{1,i}$ may be deduced directly from (14). Since each set of internal waveforms in (14) is a phase-shifted version of the set above it, it is a weighted sum of the same set of exponentials, so that no eigenvalues are necessary to express the internal waveforms which are not already expressed in the port waveforms. For a one-port measurement, (14) reduces to the formulation from [18], in which $\mathbf{S}_p[n]$ is a scalar function.

Exact solution of (14) or (15) for $\mathbf{Q}'$ (assuming a nonsingular $\mathbf{S}'_0$) results in an $\frac{mN}{2} \times \frac{mN}{2}$ matrix whose sampled time-domain behavior exactly replicates the N measured waveform samples. However, if fewer than $\frac{mN}{2}$ exponentials are required to represent the port behavior, then the problem is underdetermined. This implies that $\mathbf{S}'_0$ and $\mathbf{S}'_1$ are singular, and some of their rows can be removed before solving the problem, resulting in a smaller matrix $\mathbf{Q}$, and therefore, a smaller model.

B. Internal-Waveform Selection

Because $\mathbf{S}'_0$ and $\mathbf{S}'_1$ are contaminated with measurement noise, they generally will not be exactly singular, but instead will be nearly singular, and therefore, poorly conditioned. Any solution obtained in finite precision by inverting a near-singular $\mathbf{S}'_0$ will be extremely sensitive to small variations in $\mathbf{S}'_0$ and $\mathbf{S}'_1$, specifically to perturbations caused by measurement noise. In this paper, the problem is avoided by application of the singular-value decomposition (SVD) [19] which decomposes $\mathbf{S}'_0$ into

$$\mathbf{S}'_0 = \mathbf{U}\Sigma\mathbf{V}^T \tag{17}$$

where Σ is a diagonal matrix containing the singular values of $\mathbf{S}'_0$, $\mathbf{U}$ is an orthonormal basis for the column space of $\mathbf{S}'_0$, and $\mathbf{V}^T$ is an orthonormal basis for the row space of $\mathbf{S}'_0$. The singular values of $\mathbf{S}'_0$ provide a measure of how close the matrix is to singularity. Specifically, if exactly q singular values are larger than δ, then perturbing $\mathbf{S}'_0$ by order δ can cause all but q of its rows to become linearly dependent. It is shown in [19] that application of $\mathbf{QR}$ decomposition with column pivoting to compute an orthonormal basis for the first q rows of $\mathbf{U}^T$ indicates which q rows of $\mathbf{S}'_0$ are most linearly independent. If only these waveforms are used, (10) reduces to

$$\begin{bmatrix} \mathbf{S}'_{1,p} \\ \tilde{\mathbf{S}}_{1,i} \end{bmatrix} = \tilde{\mathbf{Q}} \begin{bmatrix} \mathbf{S}'_{0,p} \\ \tilde{\mathbf{S}}_{0,i} \end{bmatrix} \qquad \tilde{\mathbf{S}}_1 = \tilde{\mathbf{Q}}\tilde{\mathbf{S}}_0 \tag{18}$$

where the rows of $\tilde{\mathbf{S}}_{0,i}$ are those chosen by the above algorithm as being most linearly independent from each other and

from the rows of $\mathbf{S}'_{0,p}$. The corresponding rows of $\mathbf{S}'_{1,i}$ [corresponding by row number in (14)] are retained to form $\mathbf{S}_{1,i}$. Note that in the process of removing linearly dependent rows, it is important to retain the rows of $\mathbf{S}'_{0,p}$ and $\mathbf{S}'_{1,p}$, since their relationship via $\tilde{\mathbf{Q}}$ maintains the port behavior of the model.

Selection of this set of internal waveforms results in a well-conditioned linear least-squares problem, and the rows of $\tilde{\mathbf{S}}_0$ effectively span the row space of $\mathbf{S}_1$, since after a perturbation of order δ they spanned the discarded rows of $\mathbf{S}'_0$. Equation (18) may now be safely inverted via least-squares to determine $\tilde{\mathbf{Q}}$.

At this point, $\tilde{\mathbf{Q}}$ is taken to be $\mathbf{Q}$, the $M \times M$ linear prediction matrix of (6), which is the sampled version of (2), the modeling equation. To completely characterize the sampled system, $\mathbf{C}^{-1}$ must be determined. This is accomplished by noting from (7) that $\mathbf{C}^{-1} = \mathbf{S}[0]$. However, because only the first m columns of $\mathbf{S}[0]$ and $\mathbf{C}^{-1}$ are known, the additional M–m columns must be determined. Any set which preserves the conditioning of the problem is valid, and we chose

$$\mathbf{C}^{-1} = \begin{bmatrix} \mathbf{S}_p[0] & (\mathbf{S}_i[0])^T \\ \mathbf{S}_i[0] & \mu\mathbf{I} \end{bmatrix} \tag{19}$$

where μ is the two-norm of $\mathbf{S}_i[0]$.

C. Transformation to the Laplace Domain

Once $\mathbf{Q}$ and $\mathbf{C}^{-1}$ are determined, (3) and (5) are inverted to compute $\mathbf{G}$ from

$$\mathbf{X} = \frac{\log(\mathbf{Q})}{T}$$
$$\mathbf{G} = -\mathbf{C}\mathbf{X} \tag{20}$$

which completes the desired model from (1). The eigenvalues of $\log(\mathbf{Q})$ are taken as those with an imaginary part between $-\pi$ and π to limit the impulse response of the system above the Nyquist frequency π/T.

The matrix logarithm was computed via Parlett's algorithm [19]. Although a block version of the algorithm is necessary to compute $\log(\mathbf{Q})$ if the eigenvectors of $\mathbf{Q}$ tend toward linear dependence, this situation was not encountered in any examples.

D. Transformation to Admittance

If the model in (1) is built from sampled scattering impulse-response data, $\mathbf{S}(t)$ is the reflected-voltage waveforms at the ports, while the RHS is the incident-voltage waveforms. A transformation is necessary if the model is to be evaluated in an admittance-based simulator whose state variables are total voltage and current. In this paper, the entries of the extracted $\mathbf{G}$ and $\mathbf{C}$ matrices were treated as conductance and susceptance, respectively, and were entered into the SPICE simulator via a netlist of control sources and capacitors. A transformer such as that shown in Fig. 1 was placed at each port to convert the simulated total-voltage waveforms v' into reflected-voltage waveforms b, and likewise to convert simulated current waveforms i' into incident-voltage waveforms a. The transformer

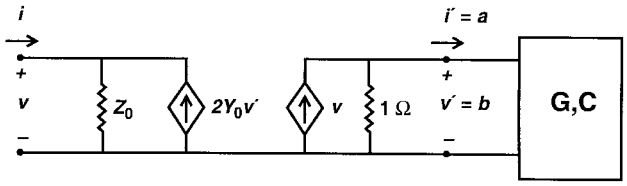

Fig. 1. Transformer for simulation of scattering-based model in admittance-based simulator.

is based on the relationship

$$v = a + b$$
$$i = Y_0(a - b). \tag{21}$$

Before the simulation netlist was actually written, a final transformation based on the eigenvectors of the system was applied to $\mathbf{G}$ and $\mathbf{C}$ to block diagonalize the lower right-hand submatrices corresponding to the internal nodes without changing the port behavior of the model. This transformation reduces simulation time by reducing the number of branches in the circuit from $O(M^2)$ to $O(M)$.

E. Asymptotic Stability and Passivity

The simulation model as derived above results in an impulse response of the form shown in (2). In the scalar sense, each element of the impulse–response matrix is an equation of the form (4). Asymptotic stability requires that the eigenvalues of $\mathbf{X}$ or poles must all have negative real parts. Although the method presented in this paper places no constraints on the extracted poles, it computes a well-conditioned set which accurately represents the data. For this reason, if the sampled data is decaying, negative poles are extracted. Any positive poles would necessarily be accompanied by very small residues so as not to destroy the fit to the data, and as such could be removed without consequence. In the examples presented in this paper, no positive poles were encountered.

Although asymptotic stability does not imply passivity, the behavior of the extracted network closely matches that of the measured passive DUT. For this reason, deviations from passivity will be small. While any deviation from passivity implies that a termination may be chosen which shifts the poles of the system into the right half-plane, if the deviation is slight, such a termination is a degenerate case, not likely to occur in an actual circuit setting. Furthermore, a frequency-dependent loss may be added to the extracted circuit to ensure passivity, although such techniques are not discussed in this paper.

F. Computational Complexity

The computational cost of the algorithm presented is primarily due to computation of the SVD in (17). Although the SVD is computed iteratively, it generally scales with the cube of the dimension of a square matrix, which translates into $O((mN)^3)$ for $\mathbf{S}'_0$ in (17). It can be seen that for a system with a large number of ports m, partial SVD techniques [19] are necessary to compute the subset of the singular values and singular vectors necessary for internal-waveform selection.

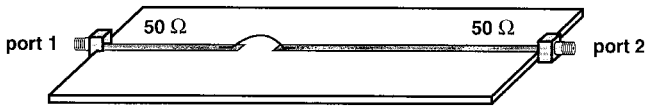

Fig. 2. Two-port microstrip example circuit. The physical distance between ports 1 and 2 is approximately 14 cm.

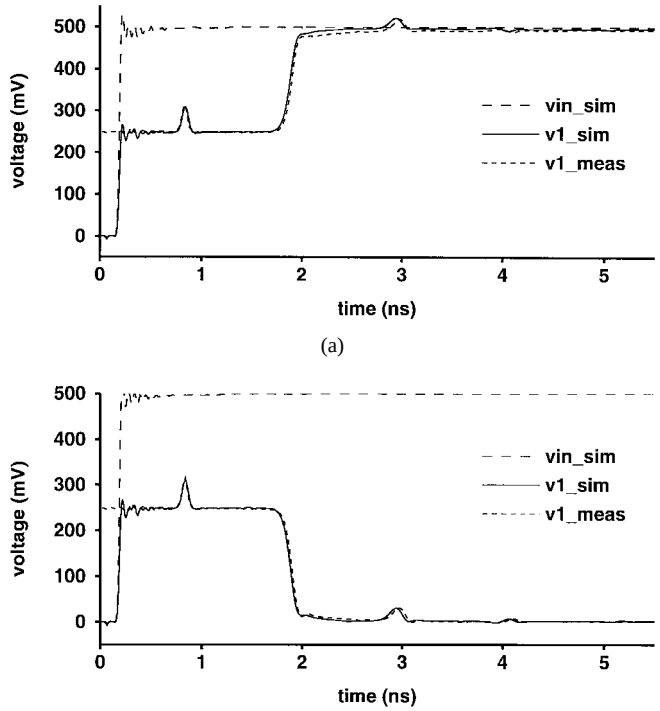

Fig. 3. Comparison of modeled and measured data for two-port example. (a) Open-circuit reflection at port 1 in response to a 35-ps step. (b) Short-circuit reflection at port 1 in response to a 35-ps step.

G. Model Reduction

In general use, the frequency content of signals incident on the circuit being modeled may fall significantly below that of the time-domain reflectometry (TDR) step. If so, it is desirable to use a simpler model that is valid over the frequency range of use to reduce simulation time. Various reduction schemes have been proposed in the literature [2]–[4]. In this paper, a reduction scheme similar to that presented in [4] was used as a post-processing step to reduce model complexity while preserving the response of the model over a requested frequency range.

IV. Examples

In this section two example circuits are characterized. The first is a two-port transmission-line circuit with an inductive discontinuity. Reflection and transmission are simulated for various independent terminations and compared with measured results. Second, a pair of tightly coupled nonuniform microstrip lines is modeled. Reflection, transmission, and crosstalk are simulated for various terminations and the results are compared with measured data.

TDR measurements were made with a Tektronix 11 801A Digital Sampling Oscilloscope and SD-24 TDR Sampling Head. The TDR is connected to the DUT by 50 $\pm$ 1 Ω, 2 $\pm$ .02-ns coaxial lines. Circuit simulations were performed using HSPICE.[1]

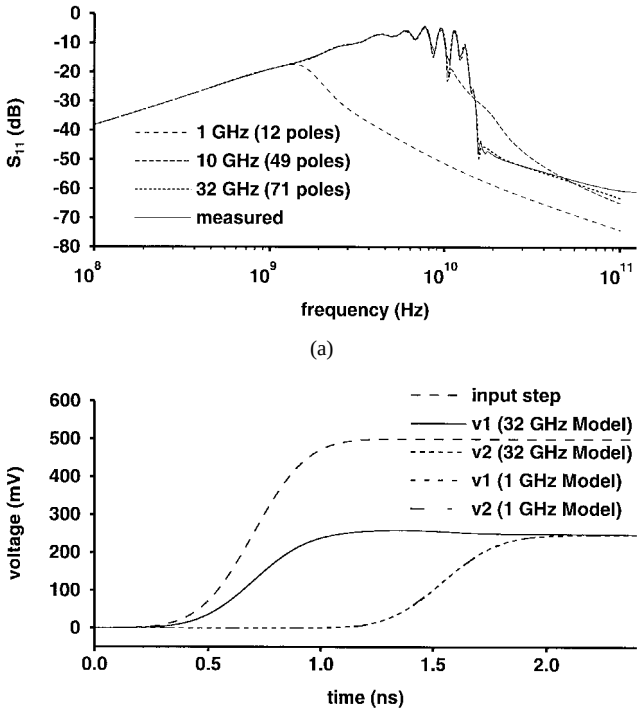

Fig. 4. Evaluation of the model of the circuit in Fig. 2. (a) Comparison of 1-, 10-, and 32-GHz reflection magnitudes at port 1 with measured data in the frequency domain. (b) Matched-load reflection at port 1 and transmission at port 2 for 1- and 32-GHz models in response to a 500-ps step.

A. Two-Port Microstrip Circuit

The two-port microstrip circuit in Fig. 2 was characterized according to the method presented in this paper. The circuit consists of two lengths of 50-Ω transmission line connected by a short piece of soldered wire, and has a 50-Ω 3.5-mm coaxial connector at each end. The physical length of the circuit is about 14 cm.

Due to the ideal delay present in the system, 69 poles were necessary to represent the four scattering parameters to within 2% accuracy up to 32 GHz. The generated SPICE netlist representing the admittance of the DUT had 71 nodes. To evaluate the accuracy of the extracted model, port 1 was driven by a 500-mV 35-ps step input through a 50-Ω output resistance, and port 2 was terminated by a resistance R_2. Fig. 3(a) compares simulated voltage at port 1 for $R_2 = 50$ $k\Omega$ with TDR data measured for port 2 unterminated. Fig. 3(b) compares simulated voltage at port 1 for $R_2 = 0.001$ Ω with TDR data measured for port 2 short circuited. Initial delay and reflection are accurately modeled in the simulated waveforms, and successive reflections due to the mismatched loads are also accurately represented.

Models were created which were accurate from dc to 1, 10, and 32 GHz. The models had 12, 49, and 71 nodes, respectively. Fig. 4(a) compares the return losses of the various

[1] *HSPICE*, Meta-Software, Inc., version H95.1, Campbell, CA, 1995.

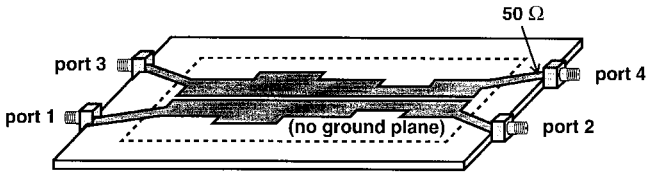

Fig. 5. Four-port microstrip example circuit. The physical distance between ports 1 and 2 is approximately 14 cm.

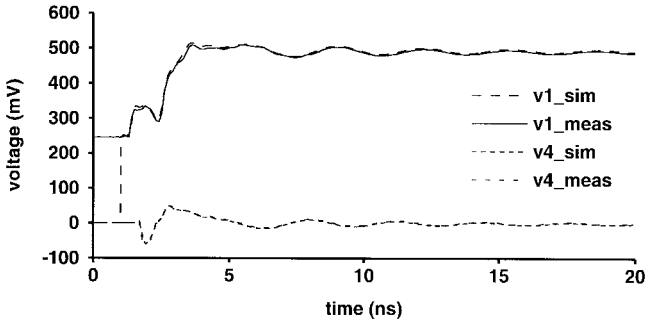

Fig. 6. Simulated and measured open-circuit reflection at port 1 and crosstalk at port 4 for the circuit in Fig. 5. Simulations were performed using the 13-GHz model and a 35-ps input step.

extracted models with that of the measured response. Fig. 4(b) compares simulated reflection at port 1 and transmission at port 2 for $R_2 = 50\ \Omega$ for the 32- and 1-GHz models in response to a 500-ps step. The two models are seen to behave identically given this excitation.

B. Four-Port Microstrip Circuit

The four-port microstrip circuit in Fig. 5 consists of two mirrored microstrip lines of varying width terminated at each end by 50-Ω SMA coaxial connectors. There is no ground plane under the majority of each trace, resulting in significant crosstalk between the two lines. The physical length of each run is about 14 cm.

A total of 148 internal nodes were required to model the 16 scattering parameters to within 2% accuracy up to 13 GHz. To demonstrate the accuracy of the model, port 1 was driven by a 500-mV 35-ps step input through a 50-Ω output impedance and port 2 was terminated by 50 $k\Omega$. Ports 3 and 4 were terminated by 50-Ω resistors. Fig. 6 compares simulation results for reflection at port 1 and crosstalk at port 4 with measured results for which port 2 was unterminated while ports three and four were matched. The simulated and measured curves are nearly overlapping at the scale shown.

Reduced models were also extracted which were accurate to within 2% up to 100 MHz, 1, and 10 GHz. These models contained 12, 23, and 103 nodes, respectively. Fig. 7 compares the magnitude of the reflection at port 1 of each model with measured data.

V. Conclusion

This paper presented a general approach for characterizing interconnect circuitry at the board, package, and MCM substrate levels using measured time-domain data. The approach begins with TDR data measured at the ports of a DUT,

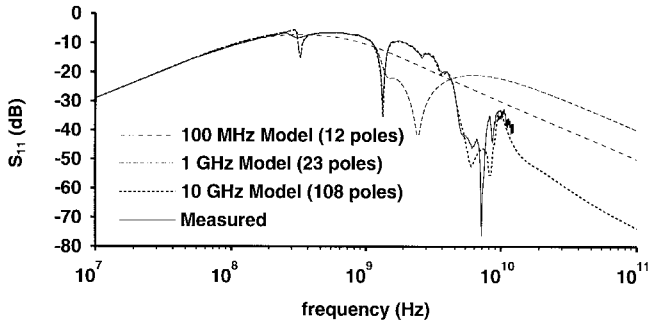

Fig. 7. Frequency-domain reflection magnitude comparison of measurement and the 100-MHz, 1-, and 10-GHz models of the circuit in Fig. 5.

and automatically extracts a SPICE subcircuit netlist whose port behavior matches that of the DUT to within a specified accuracy up to a specified frequency. Potential ill conditioning is handled rigorously and robustly. Interconnect delay and reflection, as well as crosstalk between multiple conductors of varying geometries, are modeled as accurately as they can be measured. The models are in standard SPICE format, which allows them to be evaluated in any SPICE-based simulator in conjunction with nonlinear circuitry. Two-port and four-port microstrip circuit examples were measured, characterized, and simulated, and the results were compared with measured data to demonstrate the validity of the approach.

References

[1] A. E. Ruehli and H. Heeb, "Circuit models for three-dimensional geometries including dielectrics," *IEEE Trans. Microwave Theory Tech.*, vol. 40, pp. 1507–1516, July 1992.

[2] T. J. Su and R. R. Craig, "Krylov vector methods for model reduction and control of flexible structures," *Control and Dynamic Syst.: Advances in Theory*, vol. 54, pp. 449–481, 1992.

[3] P. Feldmann and R. W. Freund, "Efficient linear circuit analysis by Padé approximation via the Lanczos process," *IEEE Trans. Computer-Aided Design*, vol. 14, pp. 639–649, May 1995.

[4] K. J. Kerns and A. T. Yang, "Preservation of passivity during RLC network reduction via split congruence transformations," presented at the *Proc. 34th Design Automation Conf.*, Anaheim, CA, June 9–13, 1997.

[5] F. H. Branin, "Transient analysis of lossless transmission lines," in *Proc. IEEE*, vol. 55, pp. 2012–2013, Nov. 1967.

[6] F. Y. Chang, "Transient analysis of lossless coupled transmission lines in a nonhomogeneous dielectric medium," *IEEE Trans. Microwave Theory Tech.*, vol. MTT-18, pp. 616–626, Sept. 1970.

[7] J. M. Jong, B. Janko, and V. Tripathi, "Equivalent circuit modeling of interconnects from time-domain measurements," *IEEE Trans. Comp., Hybrids, Manufact. Technol.*, vol. 16, pp. 119–126, Feb. 1993.

[8] S. Sercu and L. Martens, "A new algorithm for experimental circuit modeling of interconnection structures based on causality," *IEEE Trans. Comp., Packag. Manufact. Technol. B*, vol. 19, pp. 289–295, May 1996.

[9] B. J. Cooke, J. L. Prince, and A. C. Cangellaris, "S-parameter analysis of multiconductor integrated circuit interconnect systems," *IEEE Trans. Computer-Aided Design*, vol. 11, pp. 353–360, Mar. 1992.

[10] R. Kipp, C. H. Chan, A. T. Yang, and J. T. Yao, "Simulation of high-frequency integrated circuits incorporating full-wave analysis of microstrip discontinuities," *IEEE Trans. Microwave Theory Tech.*, vol. 41, pp. 848–854, May 1993.

[11] D. S. Gao, A. T. Yang, and S. M. Kang, "Accurate modeling and simulation of interconnection delay and crosstalks in high-speed integrated circuits," *IEEE Trans. Circuits Syst.*, vol. 37, pp. 1–9, Jan. 1990.

[12] G. V. Devarayanadurg and M. Soma, "An interconnect model for arbitrary terminations based on scattering parameters," *Analog Integrated Circuits Signal Processing*, vol. 5, no. 1, pp. 31–45, Jan. 1994.

[13] S. D. Corey and A. T. Yang, "Interconnect characterization using time domain reflectometry," *IEEE Trans. Microwave Theory Tech.*, vol. 43, pp. 2151–2156, Sept. 1995.

[14] _____, "Automatic netlist extraction for measurement-based characterization of off-chip interconnect," in *Proc. IEEE/ACM Int. Conf. Computer-Aided Design*, San Jose, CA, Nov. 1996, pp. 24–29.
[15] S. D. Corey, K. J. Kerns, and A. T. Yang, "Automatic characterization of lossy MCM line using lumped elements," in *Proc. IEEE 5th Topical Meeting Elect. Performance Electron. Packaging*, Napa, CA, Oct. 1996, pp. 144–146.
[16] S. Gupta, *Transform and State Variable Methods in Linear Systems*. New York: Wiley, 1966.
[17] L. A. Hayden and V. K. Tripathi, "Calibration methods for time domain network analysis," *IEEE Trans. Microwave Theory Tech.*, vol. 41, pp. 415–420, Mar. 1993.
[18] Y. Hua and T. K. Sarkar, "Matrix pencil method for estimating parameters of exponentially damped/undamped sinusoids in noise," *IEEE Trans. Acoust., Speech, Signal Processing*, vol. 38, pp. 814–824, May 1990.
[19] G. H. Golub and C. F. van Loan, *Matrix Computations*. Baltimore, MD: The Johns Hopkins Press, 1989.

Steven D. Corey received the B.S. and M.S. degrees in electrical engineering from the University of Washington, Seattle, in 1991 and 1994, respectively, and is currently working toward the Ph.D. degree in electrical engineering.

From 1994 to 1997, he worked part time at Tektronix on interconnect modeling and measurement. His research interests include numerical methods, simulation and modeling of linear interconnect, and linear network reduction.

Andrew T. Yang (S'87–M'90) received the B.S. degree in electrical engineering and computer science from the University of California at Berkeley, in 1983, and the M.S. and Ph.D. degrees from the University of Illinois at Urbana–Champaign, in 1986 and 1989, respectively.

From 1983 to 1984, he was with the Advance Micro Devices Corporation, CA. From 1989 to 1996, he was an Associate Professor of electrical engineering at the University of Washington, Seattle, where he was involved circuit simulation of mixed analog–digital circuits, timing and power simulation with emphasis on analog modeling, and modeling of semiconductor devices. In 1993, he founded Anagram, Inc., which merged with the Avant! Corporation, Fremont, CA, in 1996. He is currently the Vice President of the Analysis Products Division, Avant! Corporation, where he is responsible for the development of IC extraction, simulation, and analysis products.

Dr. Yang has served as a member of the technical program committee for the IEEE International Conference on Computer-Aided Design and the IEEE Design Automation Conference. He received the NSF Young Investigator Award (NYI) in 1992.